Direct evaluation of the local stability of structures using nonlinear FE solutions

Min-Han Oh[1,2a], Hyo-Jin Kim[1,3b], Kyungho Yoon[1,3c] and Phill-Seung Lee[*1]

*[1]Department of Mechanical Engineering, Korea Advanced Institute of Science and Technology,
291 Daehak-ro, Yuseong-gu, Daejeon 34141, Republic of Korea*
[2]Load and Response Research Department, Hyundai Heavy Industries, 75 Yulgok-ro, Jongno-gu, Seoul 03058, Republic of Korea
*[3]Center for Healthcare Robotics, Korea Institute of Science and Technology,
5 Hwarang-ro 14-gil, Seongbuk-gu, Seoul 02792, Republic of Korea*

Abstract.   In this paper, we propose three practical methods for directly evaluating stability in a local structural part of a large structure (local structure). The local stability is assessed by investigating global external load, local internal force, local strain energy, and local displacement, all calculated through nonlinear finite element (FE) analysis. A great advantage of the proposed methods is that they do not require local finite element analysis of the target local part and are applicable to arbitrarily-shaped local parts of a global structure. In addition, unlike previously developed methods, the proposed methods fully consider complicated interactions between local and global structures. The three evaluation methodologies are presented, and their practical effectiveness is demonstrated through several numerical examples.

Keywords: buckling; local stability; nonlinear finite element analysis; resistance capacity; strain energy variation

1. Introduction

To obtain high strength and excellent fracture toughness, ships and offshore structures are primarily composed of steel. However, steel members are prone to failure by local buckling because, for optimal use of materials, they are generally designed to be thin-walled. Large steel structures are built using various steel members, and thus the resistance capacity of such structures highly depends on the stability of the local members. Clearly, local stability is a crucial consideration in structural design of steel structures.

When a local part of a structure (local structure) loses stability, excessive local deformation occurs and the entire load resistance is significantly reduced. Progressive local buckling will lead to global failure of the structure. To maintain robust structural systems with desired capacity, it is important to ensure that local parts of global structures still contribute to the entire resistance. For this purpose, it is essential to accurately evaluate the critical load for local buckling. However, a global structure and its local parts are tightly connected to each other, and this makes the failure evaluation very difficult, especially for structures with complicated geometries.

The design standards for determining the resistance capacity of local parts of a large structure are based on design formulas for the buckling and ultimate strengths, which are specified in Codes and Rules (ABS 2018, AISC 2016, API 2014, BV 2018, DNV 2010, DNVGL 2015, DNVGL 2017, DNVGL 2018). However, such design formulas are only applicable to several typical shape structures such as beam-columns, rectangular stiffened plates, and cylindrical shells. Further investigations for arbitrarily-shaped local parts are required to accurately predict critical loads for local buckling.

There have been many attempts to assess the stability of local structures with various geometries. Theoretical studies have been conducted focusing on triangular and Quadrilateral plates (Jamshidi and Fallah 2019, Jaunky *et al.* 1995a, Jaunky *et al.* 1995b, Saadatpour *et al.* 1998, Tham and Szeto 1990, Wang and Liew 1994, Wu and Feng 2003, Xiang 2002, Xiang *et al.* 1994), girders, and stiffened plates (Brubak *et al.* 2007, Brubak and Hellesland 2007, Kim *et al.* 2018b, Kim *et al.* 2019). Lee *et al.* (2015) conducted a series of numerical analyses to evaluate the ultimate strength of triangular brackets in ship structures. To analyze the buckling and ultimate strengths of perforated plates, several numerical and experimental studies were carried out (Kim *et al.* 2009, Kim *et al.* 2015, Komur and Sonmez 2008, Mohammadzadeh *et al.* 2018, Muhammad and Singh 2005, Saad-Eldeen *et al.* 2016). The global failures were numerically evaluated using the theoretical local buckling modes of periodically stiffened plates commonly used in aeronautical and marine structures (Bisagni and Vescovini 2009, Wang and Abdalla 2015, Pei *et al.* 2015).

∗Corresponding author, Professor
 E-mail: phillseung@kaist.edu
[a]Senior Researcher
 E-mail: ohminhan@hhi.co.kr
[b]Postdoctoral Researcher
 E-mail: hjinkim@kist.re.kr
[c]Senior Researcher
 E-mail: kyoon@kist.re.kr

However, previously developed methods have focused on certain specific geometries. It is very difficult to distinguish the resistance capacity of an arbitrarily-shaped local part of a global structure because local behaviors are closely linked to global behaviors, but the effects of local behaviors are overshadowed by global behaviors. To overcome these limitations, Zi *et al.* separated local and global behaviors and employed nonlinear FE (finite element) analysis for a local structure (Zi *et al.* 2017). An arbitrarily-shaped bracket girder of an offshore structure was considered, but coupling between the local and global structures was ignored.

In this paper, we propose three practical methods to directly assess the stability of arbitrarily-shaped local parts of large structures considering the coupling between a target local part (local structure) and a global structure. After global nonlinear finite element analysis is performed, the local stability is assessed by investigating global load, local force, local strain energy, and local displacement. The three methods are based on the following three relations:

- Global load-local strain energy relation: The critical global load and the damaged area of the structure are evaluated through the relation between global load and strain energy stored in a target local structure.
- Global load-local force relation: The relation between global load and local force is plotted. The critical global load can be calculated. Also, the residual strength of the local structure can be evaluated through a local safety factor, which is suggested in this study.
- Local force-local displacement relation: We can confirm whether local instability is caused by so-called softening, in which deformation increases but local force decreases. This is distinguished from simple unloading, in which deformation decreases as local force decreases.

2. Practical assessments on local stability

In this section, we present three new methods for evaluating the stability in a local structural part of a large structure by using nonlinear incremental finite element analysis of the entire structure. Through the proposed methods, the critical load at which the target local structure loses its stability is predicted. In addition, safety margin, damaged area, and deformation characteristics of the target local structure can be investigated.

Consider a target local part Ω_L (local structure) in a large structure subjected to external load $\boldsymbol{f}^g$ and displacement boundary conditions as shown in Fig. 1. To evaluate the stability of the target local structure, nonlinear incremental analysis is performed with multiple load steps for the entire structure. The following incremental equilibrium equation is solved using the Newton-Raphson scheme at each load step i

$$\boldsymbol{K}_i \Delta \boldsymbol{u}_i = \boldsymbol{f}_i^g - \boldsymbol{f}_i^{int} \quad \text{with } \boldsymbol{u}_i = \boldsymbol{u}_{i-1} + \Delta \boldsymbol{u}_i, \quad (1)$$

where $\boldsymbol{K}_i$ is the tangential stiffness matrix, $\Delta \boldsymbol{u}_i$ is the incremental displacement vector, $\boldsymbol{f}_i^g$ is the global external load vector, $\boldsymbol{f}_i^{int}$ is the internal force vector, and $\boldsymbol{u}_i$ is the
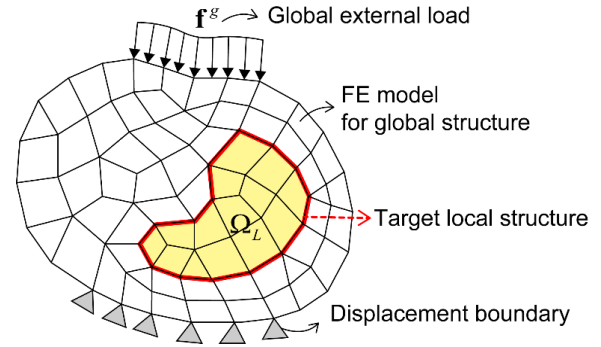

Fig. 1 Finite element model for global structure including target local structural part Ω_L. The red line represents the interface boundary between the local and global structures

displacement vector at load step i.

In Eq. (1), the global external load vector $\boldsymbol{f}_i^g$ at load step i can be represented by using global reference external load $\boldsymbol{f}_r^g$ and global load ratio λ_i^g

$$\boldsymbol{f}_i^g = \lambda_i^g \boldsymbol{f}_r^g \quad \text{with } \boldsymbol{f}_r^g = \frac{\boldsymbol{f}^g}{N}, \quad (2)$$

where N is a sufficiently large number such that the structural behavior is within the linear response region with the global reference external load $\boldsymbol{f}_r^g$.

Utilizing the results of the nonlinear incremental FE analysis for the entire structure at each load step i, the stability of the target local structure is evaluated.

2.1 Global load-local strain energy relation and identification of damaged areas

First, we introduce a method to determine the critical global load and damaged area in the target local structure using the relationship between the global external load and the strain energy stored in the target local structure.

The Lagrange-Dirichlet theorem states that the equilibrium state of a conservative system is determined by evaluating the sign of the second variation of the total potential energy Π, as follows (Bazant and Cedolin 1991)

$$\delta^2 \Pi \begin{cases} > 0, \text{Positive (stable equilibrium)} \\ = 0, \text{Zero (neutral equilibrium)} \\ < 0, \text{Negative (unstable equilibrium)} \end{cases} \quad (3)$$

Based on this theorem, the stability of a local structural part in a large structure can be evaluated using the second variation of the strain energy stored in the local structure.

Let us consider a structure at load step i as shown in Fig. 2(a). The second variation of the strain energy in the target local structure Ω_L is calculated using the following equation

$$\delta^2 \Pi_i \simeq \frac{1}{2} \Delta \boldsymbol{f}_i^l \cdot \Delta \boldsymbol{u}_i^l, \quad (4)$$

where $\Delta \boldsymbol{f}_i^l$ and $\Delta \boldsymbol{u}_i^l$ denote the distributions of incremental internal force and incremental displacement along the interface boundary of the target local structure (red line in Fig. 2(a)).

Using Eq. (4), the relation between $\delta^2 \Pi_i$ and the global
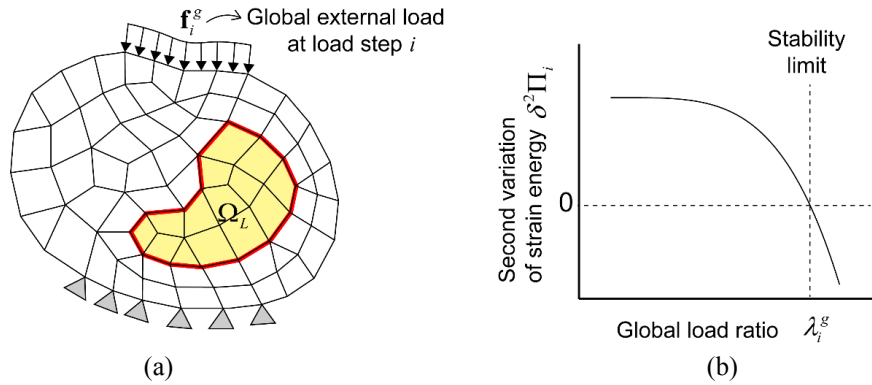
Fig. 2 Finite element model and second variation of strain energy at load step i: (a) target local structure (colored in yellow) when global structure is subjected to $\boldsymbol{f}_i^g$ and (b) relationship between global load ratio (λ_i^g) and second variation of strain energy ($\delta^2 \Pi_i$)
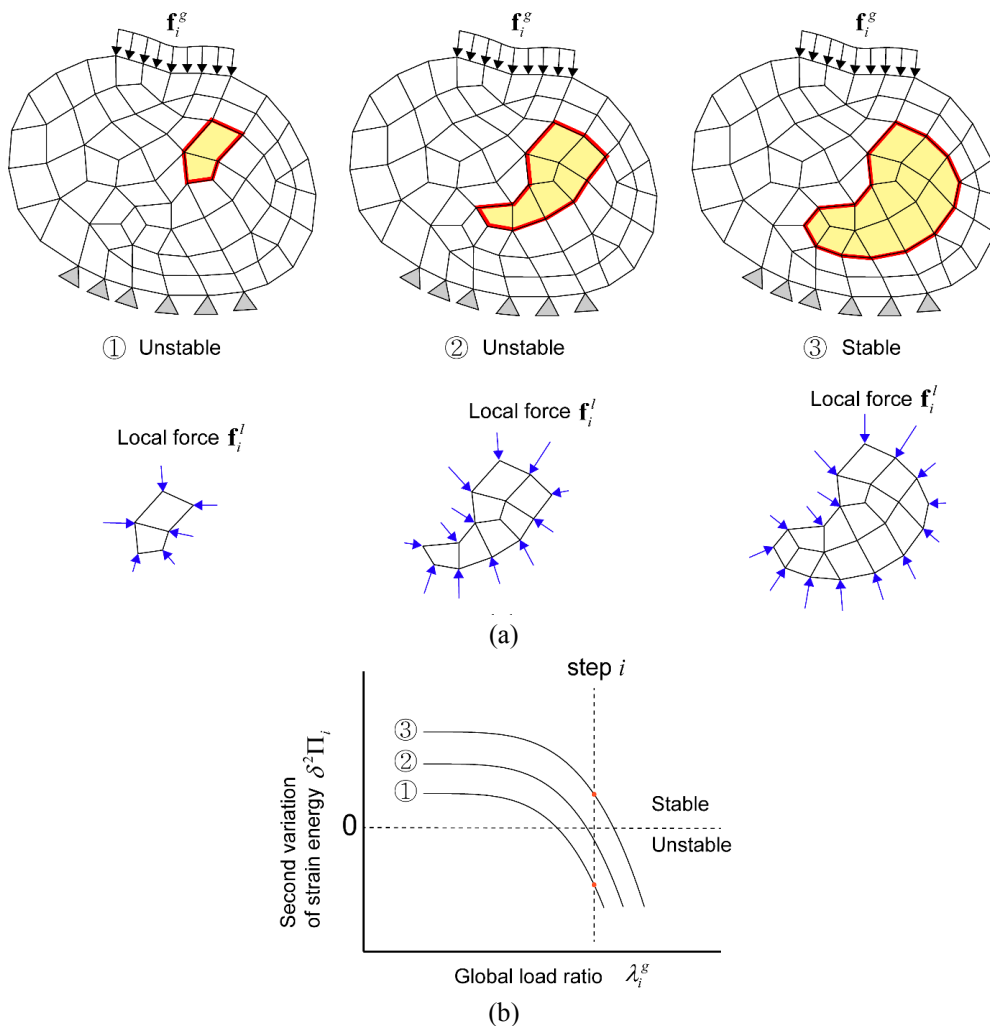

Fig. 3 Identification of damaged area in target local structure: (a) evaluation process of damaged area and (b) global load ratio (λ_i^g) - second variation of strain energy ($\delta^2 \Pi_i$) curves for cases ①, ②, and ③

load ratio λ_i^g at load step i is obtained as illustrated in Fig. 2(b). When $\delta^2 \Pi_i = 0$, the target local structure loses its stability, and the critical global external load can be calculated from the global load ratio at this point.

The damaged area in the target local structure is determined by using the strain energy stored in the finite elements of the FE model. First, we calculate the second variation of strain energy $\delta^2 \Pi_i^{(e)}$ for each element e constituting the target local structure. Starting from the area that consists of unstable elements where $\delta^2 \Pi_i^{(e)} < 0$ (① in Fig. 3(a)), we calculate the sum of $\delta^2 \Pi_i^{(e)}$ in the area (② in Fig. 3(a)) while gradually expanding the considered
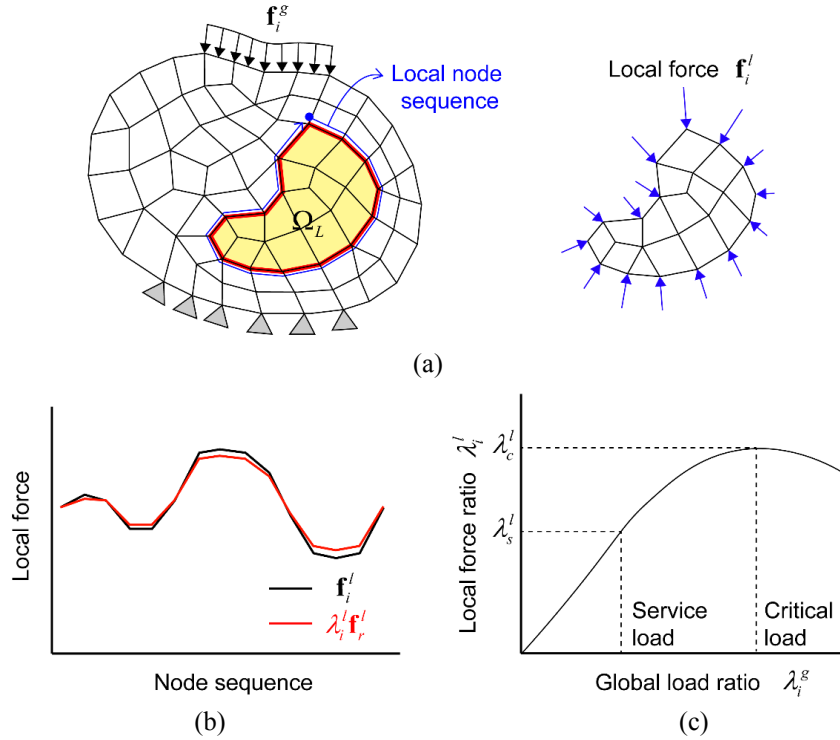
Fig. 4 Finite element models and local force ratios: (a) local node sequence of target local structure when global structure is subjected to $\boldsymbol{f}_i^g$, (b) approximation of local force distribution along local node sequence using $\lambda_i^l \boldsymbol{f}_r^l$, and (c) local force ratio at service and critical loads

area to include the surrounding elements. The extent at the step immediately before, when $\sum_e \delta^2 \Pi_i^{(e)} > 0$ (③ in Fig. 3(a)), becomes the damaged area in the target local structure. Fig. 3(b) illustrates the global load ratio (λ_i^g) - second variation of strain energy ($\delta^2 \Pi_i$) curves for cases ①, ②, and ③.

Since the proposed method requires only the strain energy values calculated during the FE analysis of the whole structure, the target local part can be easily switched without additional FE analysis. By partially reinforcing the identified damaged area in the target local structure, the strength of the entire structure can be reinforced cost-effectively.

2.2 Global load-local force relation and local safety factor

Second, we introduce a method to determine the critical global load and local safety factor (*LSF*) from the relationship between the global external load and the local force at the interface boundary of the target local structure.

When global external load $\boldsymbol{f}_i^g$ is applied to the whole structure at load step i, the interface boundary of the target local structure is subjected to local force $\boldsymbol{f}_i^l$, as shown in Fig. 4(a). By employing the local force ratio λ_i^l, the local force $\boldsymbol{f}_i^l$ at load step i can be approximated as

$$\boldsymbol{f}_i^l \simeq \lambda_i^l \boldsymbol{f}_r^l, \tag{5}$$

where the local reference force $\boldsymbol{f}_r^l$ denotes the force at the interface boundary of the target local structure when the

global reference load $\boldsymbol{f}_r^g$ is acting on the structure.

When the structural behavior is linear, the magnitude of the local force $\boldsymbol{f}_i^l$ changes in proportion to the increase in the global reference load $\boldsymbol{f}_r^g$, while the shape of the local force distribution remains the same. However, in cases in which structure exhibits nonlinear behavior, the shape of the local force distribution changes as the global reference load $\boldsymbol{f}_r^g$ increases due to load redistribution inside the structure.

For this reason, local force $\boldsymbol{f}_i^l$ at load step i needs to be approximated using the least square fitting method, with the following squared error function φ_i

$$\varphi_i = \left(\boldsymbol{f}_i^l - \lambda_i^l \boldsymbol{f}_r^l\right) \cdot \left(\boldsymbol{f}_i^l - \lambda_i^l \boldsymbol{f}_r^l\right), \tag{6}$$

where λ_i^l is the local force ratio.

The error function in Eq. (6) is minimized when local force ratio λ_i^l becomes

$$\lambda_i^l = \frac{\boldsymbol{f}_i^l \cdot \boldsymbol{f}_r^l}{\boldsymbol{f}_r^l \cdot \boldsymbol{f}_r^l}, \tag{7}$$

and the local force $\boldsymbol{f}_i^l$ can be approximated using the local force ratio λ_i^l in Eq. (7) with the local reference force $\boldsymbol{f}_r^l$, as depicted in Fig. 4(b).

Fig. 4(c) illustrates the relation between the local force ratio λ_i^l and the global load ratio λ_i^g at load step i. The point at which the global load ratio λ_i^g increases but the local force ratio λ_i^l begins to decrease becomes the critical point for the target local structure. The critical point indicates that the target local structure can no longer withstand the load transmitted from the surrounding areas. The local force ratio at this point becomes the critical local
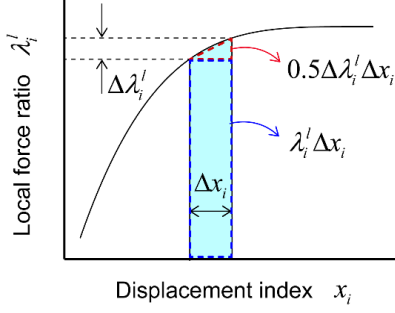
Fig. 5 Relationship between displacement index (x_i) and local force ratio (λ_i^l)

force ratio (λ_c^l).

When the structure is subjected to a service load $\boldsymbol{f}_s^g$, a usage factor η for the target local structure is obtained as

$$\eta = \frac{\lambda_s^l}{\lambda_c^l} \text{ with } 0 \leq \eta \leq 1, \tag{8}$$

where λ_s^l is the local force ratio corresponding to the service load.

The local safety factor (LSF) value, which represents the degree of safety in the target local structure, is defined as the reciprocal value of the usage factor

$$LSF = \frac{1}{\eta}. \tag{9}$$

The larger the LSF value, the more safety in the target local structure is guaranteed.

Unlike previously developed methods that did not consider effects of interactions between the target local structure and the surrounding global structure, the proposed method is based on FE analysis of the entire structure, including interactions between them. This makes it possible to provide a more accurate and reasonable evaluation of the safety margin and residual strength of the target local structure.

2.3 Local force-local displacement relation and deformation characteristics

Finally, we introduce a method to determine the critical

global load and deformation characteristics of a local structure through the relationship between the local force and the displacement of the local structure. To represent the magnitude of the displacement in the target local structure as a single variable, displacement index x_i is calculated from the incremental strain energy at each load step i. That is, the local deformation is measured by a single value x_i.

Assuming that the strain energy is a function of the variable x_i, the incremental strain energy ΔU_i at load step i is obtained by using the 2nd order Taylor expansion

$$\Delta U_i = U(x_i + \Delta x_i) - U(x_i) \simeq \frac{dU}{dx_i}\Delta x_i + 0.5\frac{d^2U}{dx_i^2}\Delta x_i^2, \tag{10}$$

where Δx_i is the incremental displacement index at load step i.

The derivative of the strain energy at load step i in Eq. (10) with respect to x_i is approximated using the local reference force $\boldsymbol{f}_r^l$ and local force ratio λ_i^l

$$\frac{dU}{dx_i} = |\boldsymbol{f}_i^l| \simeq \lambda_i^l|\boldsymbol{f}_r^l|. \tag{11}$$

Substituting Eq. (11) into Eq. (10), the following equation is obtained

$$\Delta U_i \simeq \lambda_i^l\Delta x_i|\boldsymbol{f}_r^l| + 0.5\frac{d\lambda_i^l}{dx}\Delta x_i^2|\boldsymbol{f}_r^l|. \tag{12}$$

Substituting the derivative of the local force ratio ($\frac{d\lambda_i^l}{dx_i}$) in Eq. (12) for an incremental term ($\frac{\Delta\lambda_i^l}{\Delta x_i}$), we obtain

$$\Delta U_i \simeq \left(\lambda_i^l\Delta x_i + 0.5\Delta\lambda_i^l\Delta x_i\right)|\boldsymbol{f}_r^l|. \tag{13}$$

From Eq. (13), the incremental displacement index Δx_i is obtained

$$\Delta x_i = \frac{\Delta U_i}{|\boldsymbol{f}_r^l|(\lambda_i^l + 0.5\Delta\lambda_i^l)}, \tag{14}$$

and the displacement index x_i at each load step i is calculated by the total sum of Δx_i

$$x_i = \sum_i \Delta x_i. \tag{15}$$

Fig. 5 shows the relation between the displacement index (x_i) and local force ratio (λ_i^l) at load step i. The area shaded in blue in Fig. 5 graphically represents the term
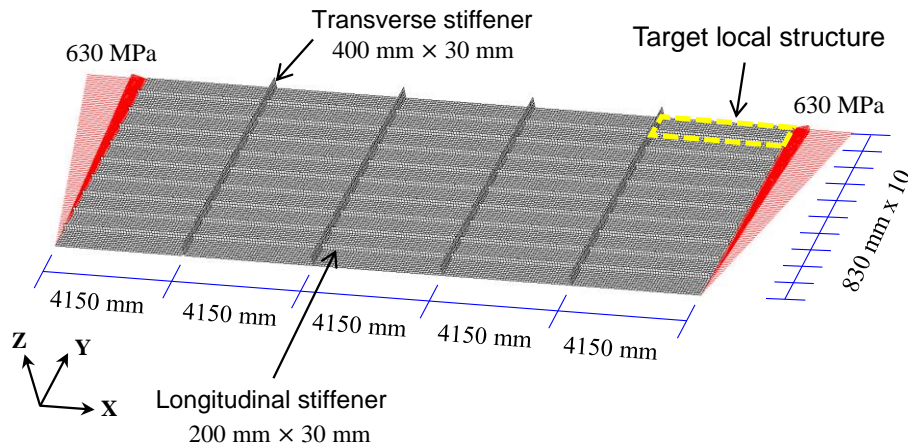

Fig. 6 FE model of simply supported stiffened rectangular plate structure with 4 and 9 stiffeners in *X*- and *Y*-directions
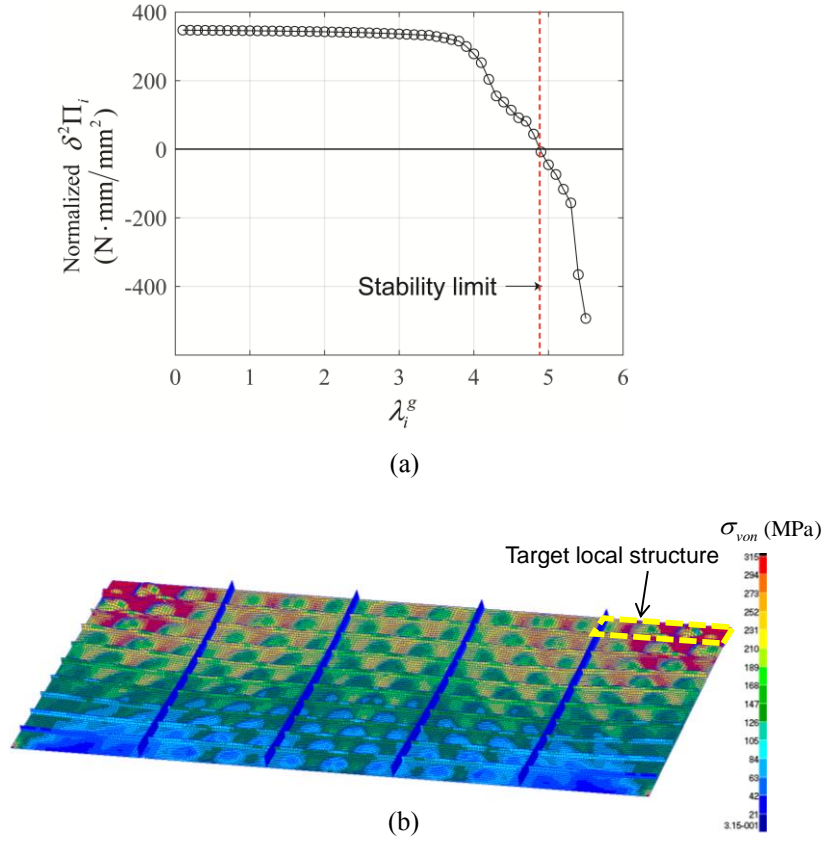
(a)

(b)

Fig. 7 Stability limit determined by relation between global load ratio and second variation of strain energy and stress distribution at the critical point: (a) Normalized second variation of strain energy of target local structure and (b) von Mises stress distribution over deformed shape of entire plate at $\lambda_i^g = 4.85$
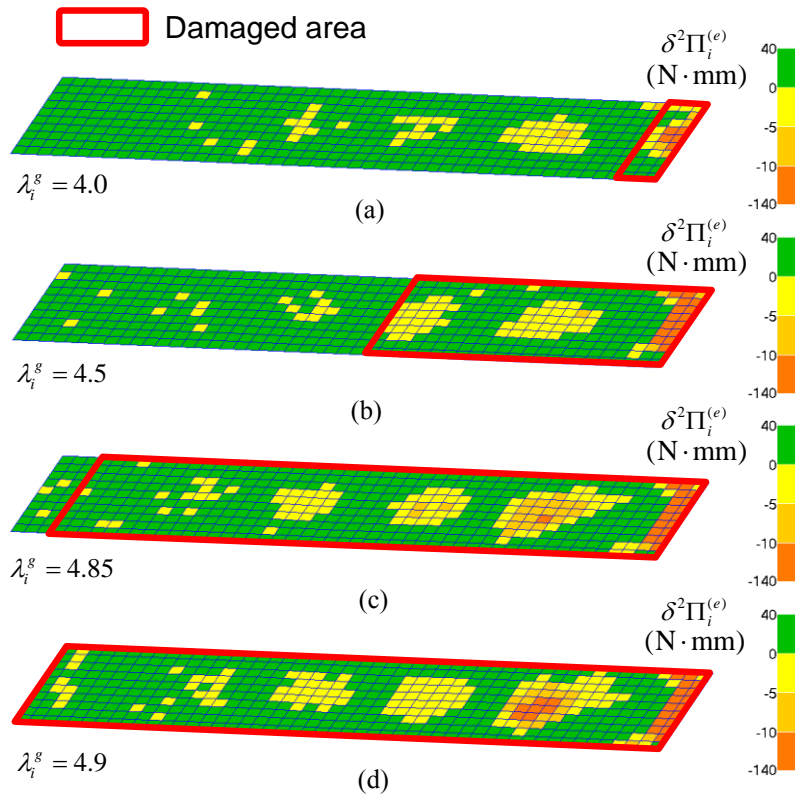

(a)

(b)

(c)

(d)

Fig. 8 Distributions of second variation of strain energy in target local structure: (a) when $\lambda_i^g = 4.0$, (b) $\lambda_i^g = 4.5$, (c) $\lambda_i^g = 4.85$, and (d) $\lambda_i^g = 4.9$
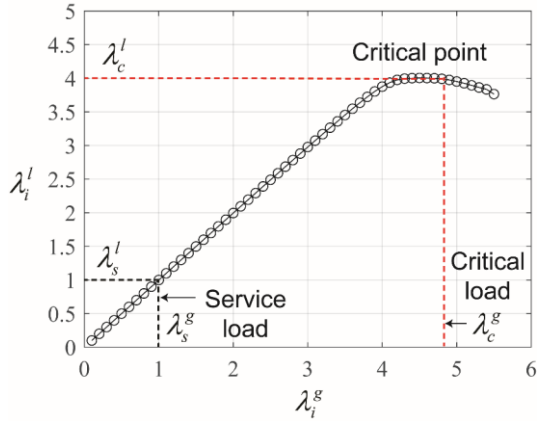
Fig. 9 Global load ratio-local force ratio curve obtained for stiffened rectangular side-wall plate problem
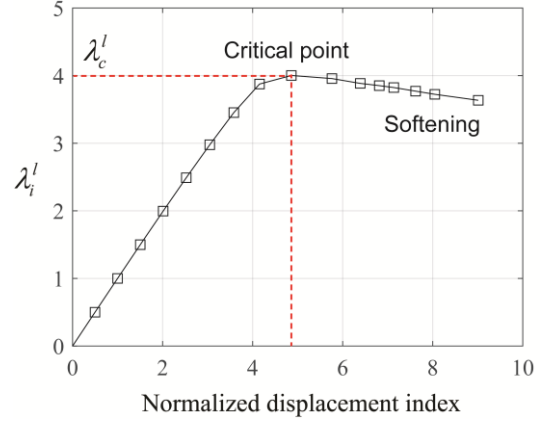
Fig. 11 Normalized displacement index-local force ratio curve obtained for stiffened rectangular side-wall plate
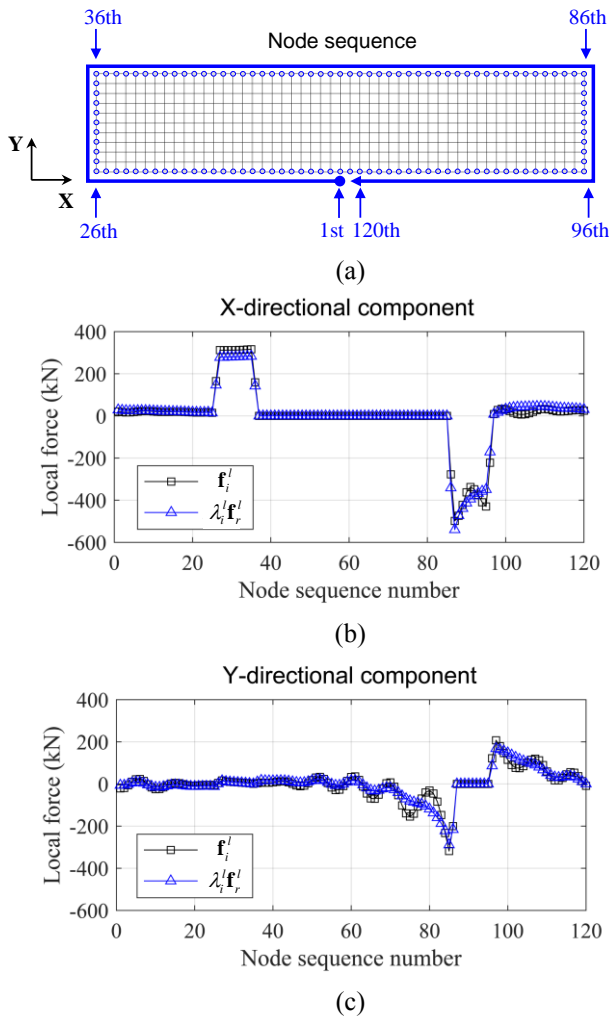

(a)

(b)

(c)

Fig. 10 Comparisons between applied and approximated local forces in stiffened rectangular side-wall plate: (a) node sequence over interface boundary of target local structure, (b) *X*-directional components of applied and approximated local forces, and (c) *Y*-directional components of applied and approximated local forces

$(\lambda_i^l \Delta x_i + 0.5 \Delta \lambda_i^l \Delta x_i)$ in Eq. (13). The point at which the value of the local force ratio λ_i^l does not increase even

though displacement index x_i increases becomes the critical point. The proposed method has the advantage of not only being able to evaluate the critical point for the target local structure, but also being able to determine the deformation characteristics by examining the displacement index at each load step. It is possible to distinguish whether local instability is due to softening or unloading. In the softening case, the displacement index increases but the local force decreases. In the unloading case, the displacement index decreases as the local force decreases.

3. Illustrative examples

To demonstrate the proposed methods, we here present three numerical examples regarding practical engineering problems: a stiffened rectangular plate, a stiffened cylindrical shell structure, and a column-pontoon connection structure in a tension leg platform. FE models are constructed using 3- and 4-node shell elements (Lee and Bathe 2005, Lee *et al*. 2007, Lee and Bathe 2010, Lee *et al*. 2014, Jeon *et al*. 2014, Jeon *et al*. 2015, Ko *et al*. 2016, Ko *et al*. 2017), and the nonlinear equilibrium equations are iteratively solved by the Newton-Raphson method (MSC Software 2018).

For each problem, the second variation of strain energy ($\delta^2 \Pi_i$) in the target local structure is calculated at each load step i, and the relation between the global load and local force ratios is plotted to determine the critical point. Using the critical values, the usage factor η and local safety factor (LSF) are obtained. Also, the displacement indexes x_i are calculated at each load step i to investigate the deformation characteristics.

In actual incremental nonlinear analysis, the load step size varies and thus the normalization of the second variation of strain energy by $\delta^2 \Pi_i / (\Delta \boldsymbol{u}_i^l \cdot \Delta \boldsymbol{u}_i^l)$ is necessary. The displacement index is also normalized as $\frac{x_i}{x_r}$, where x_r is the displacement index value when the reference global load is applied.

The results obtained from the proposed methods are compared with those by the local FE analysis method (Zi *et al*. 2017) and the design rule (DNV 2010). Zi *et al*.
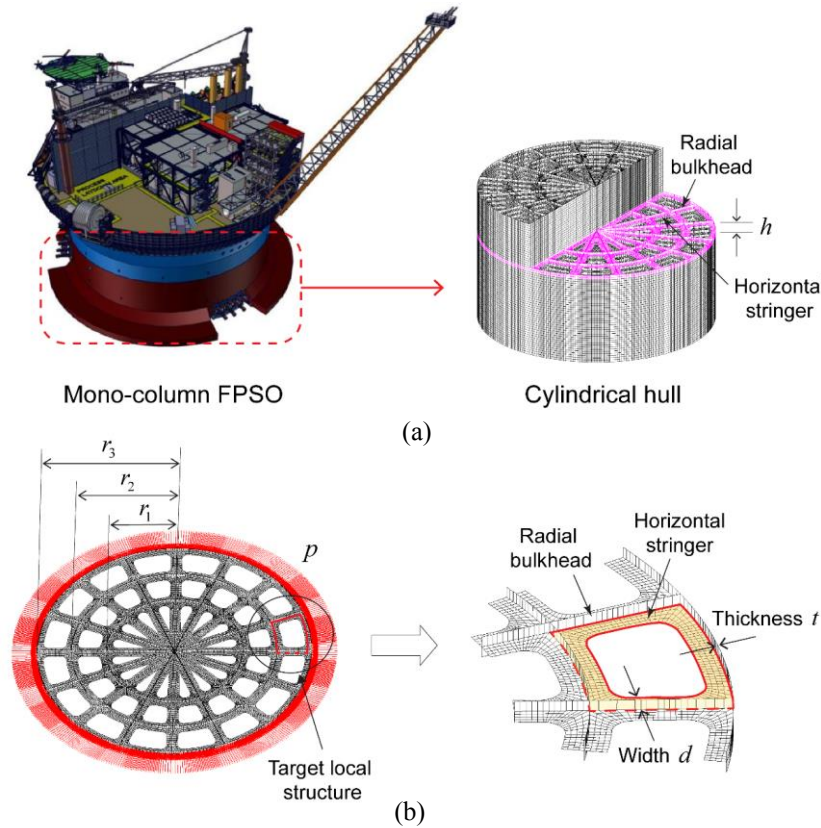
Fig. 12 FE model of stiffened cylindrical shell structure: (a) cylindrical hull structure in mono-column FPSO (floating production storage and offloading) unit and (b) stiffened cylindrical shell structure of height

proposed a usage factor to measure the safety of local structures of non-typical geometry. The basic idea is to extract the local structure from the global structure and to perform nonlinear analysis of the local structure subjected to prescribed interface displacements. The usage factor is evaluated using the strain energies stored in the local structure.

3.1 Stiffened rectangular side-wall plate

We consider a stiffened rectangular side-wall plate, shown in Fig. 6, which has been widely used in ship structures. To simulate a plate subjected to hull girder bending condition, a linearly distributed load of 630 MPa is incrementally applied to both the left and right edges of the plate. The initial imperfection is applied as the form of five half sine waves in the longitudinal direction (X-direction) with maximum out-of-plane (Z-direction) deflections of 5.73 mm (Kim *et al*. 2018a). The four edges of the plate are simply supported, and the constraint conditions are applied to them to enforce the straight edges during deformation. The plate is made of elastic-perfectly plastic high-tensile steel with Young's modulus $E = 205.8$ GPa, Poisson's ratio $\nu = 0.3$, and yield stress $\sigma_y = 315$ MPa.

An area corresponding to 1/50 of the entire plate is chosen as the target local structure (see the area marked with a yellow line in Fig. 6). The reference global load $\boldsymbol{f}_r^g$ is selected as 1/10 of the final applied load (630 MPa).

Note that, for the calculation of the usage factor and local safety factor, it is convenient to set the reference global load equal to the service load. The entire plate is modeled using 31,100 4-node shell elements, and incremental finite element analysis is performed.

To assess the local stability of the plate structure, the normalized second variations of strain energy corresponding to the target local structure are calculated at each global load ratio λ_i^g (see Fig. 7(a)). From Fig. 7(a), we can observe that the local structure is stable until the global load ratio reaches about $\lambda_i^g = 4.85$. Fig. 7(b) shows the distribution of the von Mises stress over the deformed shape of the plate structure at $\lambda_i^g = 4.85$.

Figs. 8(a)-(d) show the distributions of the second variation of the strain energy calculated over the target local structure when the global load ratios are $\lambda_i^g = 4.0$, 4.5, 4.85, and 4.9. The damaged area is determined at each load step i by evaluating the sum of the second variation of the strain energy in the local area. The damaged area propagates from the right side of the target local structure, and gradually increases as the global external load increases (Figs. 8(b)-(c)). Finally, the target local structure is fully damaged at $\lambda_i^g = 4.9$ (Fig. 8(d)).

The local force ratios λ_i^l corresponding to the global load ratio λ_i^g at each load step i are plotted in Fig. 9. The critical global load ratio and critical local force ratio can be determined as $\lambda_c^g = 4.85$ and $\lambda_c^l = 4.0$, respectively. Fig. 10(a) shows the node sequence over the interface boundary

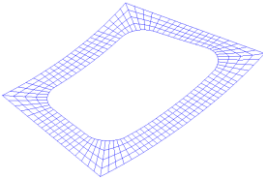Table 1 Local safety factors calculated for local plate structure in ship-shaped structure

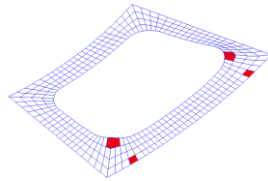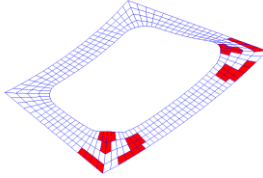|	
Direct evaluation through global FE analysis (Proposed)	4.00
Evaluation through local FE analysis (Zi *et al.* 2017)	6.67
Design formula (DNV 2010)	4.26
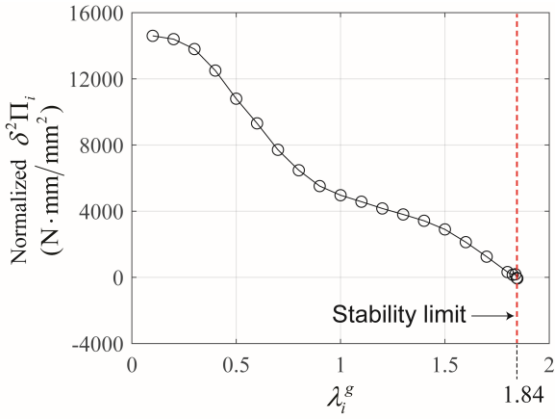
(a)

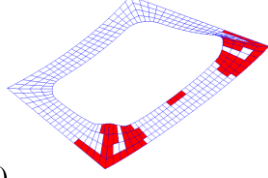■ Plastic region

$p = 1.0$ MPa $p = 1.5$ MPa

$p = 1.7$ MPa $p = 1.84$ MPa

(b)

Fig. 13 Stability limit determined by relation between global load ratio and second variation of strain energy and stress distribution at critical point, and plastic deformations in target local structure: (a) normalized second variation of strain energy of target local structure and (b) plastic regions over deformed shapes of target local structure when external pressure loads are $p = 1.0$ MPa, 1.5 MPa, 1.7 MPa, and 1.84 MPa

of the target local structure. Figs. 10(b)-(c) compare the components of the applied local force ($\boldsymbol{f}_i^l$) and the approximated local force ($\lambda_i^l \boldsymbol{f}_r^l$) on the nodes at the critical point. The approximated local force calculated using the proposed method exhibits good agreement with the applied local force.

Assuming that the service load ratio λ_s^l is equal to 1.0, the usage factor and local safety factor (LSF) are calculated using Eqs. (8) and (9) as $\eta = 0.25$ and $LSF = 4.0$. Table 1 compares the local safety factors obtained from the proposed method, the design rule (DNV 2010), and the local FE analysis method (Zi *et al.* 2017). The proposed
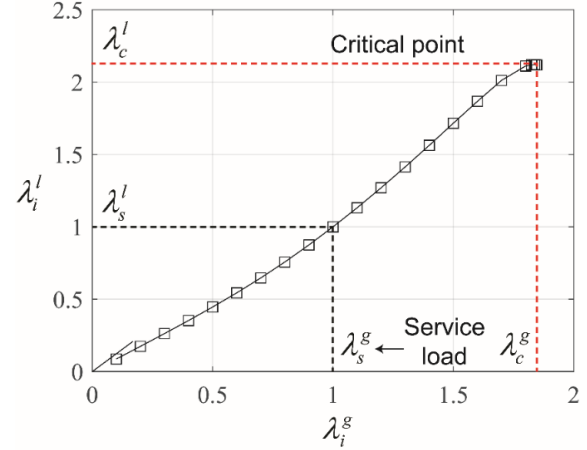

Fig. 14 Global load ratio-local force ratio curve obtained for stiffened cylindrical shell structure

method and the design rule provide similar *LSF* values, while the local FE analysis method produces a substantially larger LSF value.

To investigate the deformation characteristics of the local structure near the critical point, the displacement indexes x_i are calculated at each load step i. Fig. 11 shows the normalized displacement index-local force ratio curve. Softening slightly occurs in the target local structure after the local force ratio reaches the critical point ($\lambda_c^l = 4.0$).

3.2 Stiffened cylindrical shell structure

We consider a stiffened cylindrical shell structure of height $h = 1.0$ m, the part of the main hull in a mono-column FPSO (floating production storage and offloading) unit (Lei *et al.* 2018), as shown in Figs. 12(a). The hull structure is stiffened by radial bulkheads and horizontal stringers to resist external pressure loads. The outer and inner radii of the considered cylindrical shell structure are $r_1 = 25$ m, $r_2 = 37.5$ m, and $r_3 = 50$ m respectively; the width of the stringer is $d = 2.0$ m, and the thicknesses of all the members are $t = 0.06$ m. The hull is made of elastic-perfectly plastic high-tensile steel with Young's modulus $E = 210$ GPa, Poisson's ratio $\nu = 0.3$, and yield stress $\sigma_y = 355$ MPa. Uniform static pressure load $p = 10$ MPa is incrementally applied to the external area of the hull.

The local area that consists of horizontal stringers is chosen as the target local structure (see the marked area in Fig. 12(b)). The entire cylindrical shell structure is modeled using 24,128 4-node shell elements over a 0.5 m $\times$ 0.5 m element size. To apply the initial imperfection, the model geometry is modified by adding the first buckling mode shape, obtained from eigenvalue analysis, with a maximum deflection of 10.0 mm. The reference global load $\boldsymbol{f}_r^g$ is selected as $1/10$ of the final applied load ($p = 1.0$ MPa).

Fig. 13(a) shows the normalized second variation of the strain energy corresponding to the target local structure calculated at each global load ratio λ_i^g. The target local structure is stable until the global load ratio reaches $\lambda_i^g =$
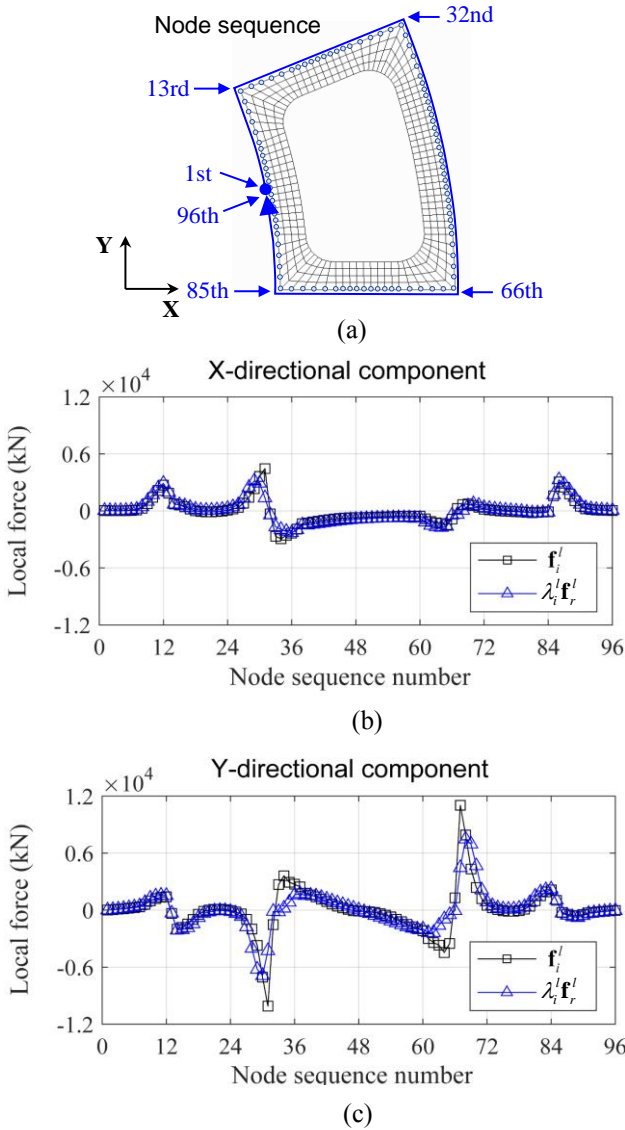
(a)

(b)

(c)

Fig. 15 Comparison between applied and approximated local forces in stiffened cylindrical shell structure: (a) node sequence over interface boundary of target local structure, (b) *X*-directional components of applied and approximated local forces, and (c) *Y*-directional components of applied and approximated local forces

1.84 ($p = 1.84$ MPa). Fig. 13(b) shows the deformed shapes and plastic regions in the target local structure when the external pressure loads are $p = 1$ MPa, 1.5 MPa, 1.7 MPa, and 1.84 MPa. The first yielding occurs at $p = 1.5$ MPa; most of the corner areas directly subjected to pressure loads become plastic at $p = 1.84$ MPa.

Fig. 14 shows the local force ratio (λ_i^l) with respect to the global load ratio (λ_i^g) at each load step i. The global load and local force ratios at critical point can be determined as $\lambda_c^g = 1.84$ and $\lambda_c^l = 2.12$, respectively. Figs. 15(a)-(c) show the nodal sequence over the boundary of the target local structure, and the components of the applied local force ($\mathbf{f}_i^l$) and the approximated local force $\lambda_i^l \mathbf{f}_r^l$ at the critical point.

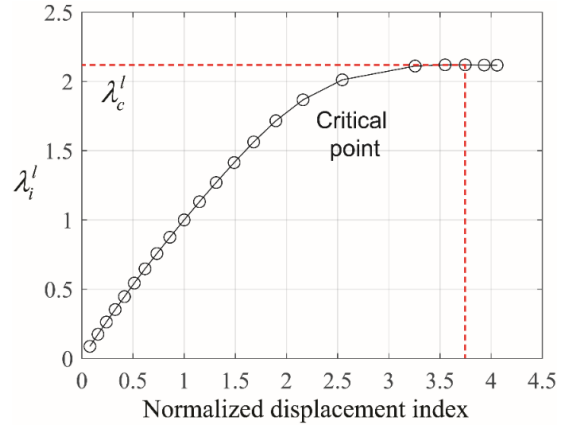For the service load ratio $\lambda_s^l = 1.0$, the usage factor and

Fig. 16 Global load ratio-local force ratio curve obtained for stiffened cylindrical shell structure

Table 2 Local safety factors calculated for local stringer structure in stiffened cylindrical structure

Direct evaluation through global FE analysis (Proposed)	2.12
Evaluation through local FE analysis (Zi *et al.* 2017)	2.84

local safety factor are calculated using Eqs. (8) and (9) as $\eta = 0.47$ and $LSF = 2.12$, respectively. Table 2 compares the local safety factors obtained from the present method and the local FE analysis method (Zi *et al.* 2017). Evaluation through local FE analysis shows a much higher safety factor than the proposed method. Note that the local FE analysis method provides local safety calculated using strain energies stored in the local structure.

Fig. 16 shows the normalized displacement index-local force ratio curve. The local force ratio does not decrease after the local force ratio reaches the critical point ($\lambda_c^l = 2.12$).

3.3 Column-pontoon connection structure in tension leg platform

We consider a column-pontoon connection structure in a tension leg platform (TLP), as shown in Fig. 17(a) (Blarez 2018). The main part of the TLP structure consists of four cylindrical columns on box-type pontoons. To stiffen the connection between the cylindrical columns and pontoons, bracket girders are used as shown in Fig. 17(b). Assuming the TLP structure is installed in a calm sea, we consider uniformly distributed external seawater pressure and internal tank pressure. The material properties of the column-pontoon connection structure are approximated as elastic-perfectly plastic high-tensile steel with Young's modulus $E = 210$ GPa, Poisson's ratio $\nu = 0.3$, and yield stress $\sigma_y = 355$ MPa.

The bracket girder is selected as the target local structure. The bracket girder has non-typical geometry. Note that it is not possible to evaluate the local stability of the bracket girder using existing design formulas. The considered column-pontoon connection structure is modeled using 39,772 3- and 4-node shell elements. To apply the initial imperfection, the geometry of the FE model is modified by adding a buckling mode shape obtained from
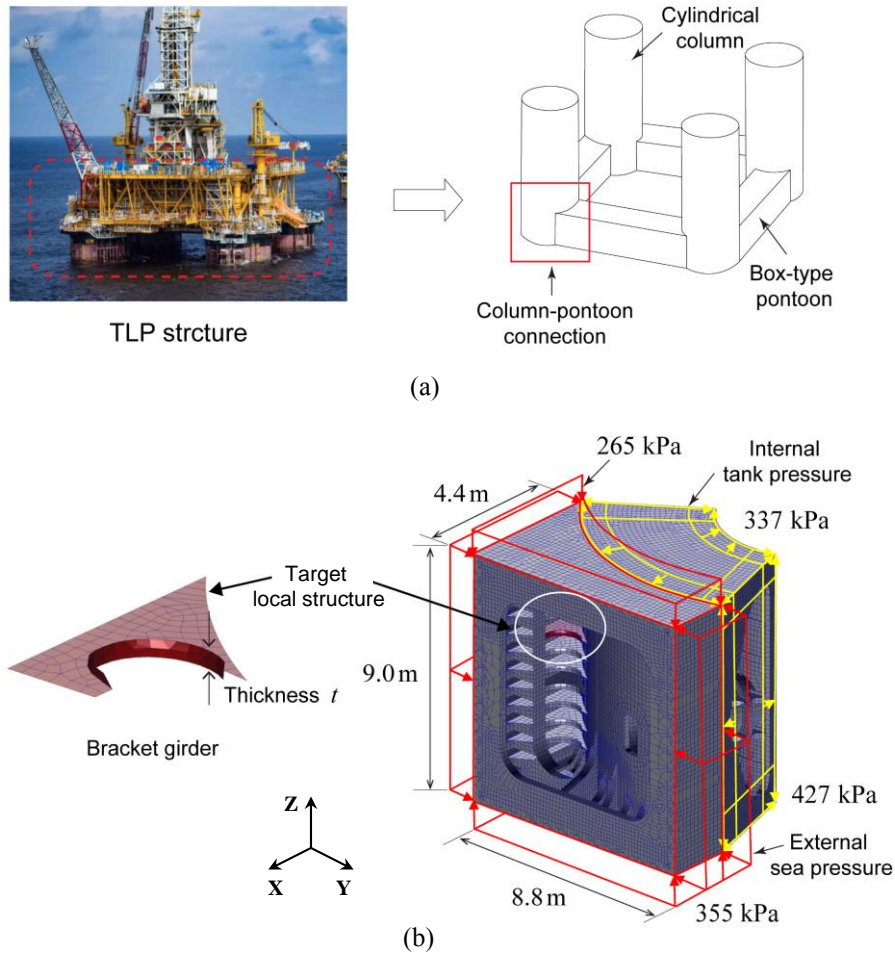
(a)

(b)

Fig. 17 FE model of column-pontoon connection structure: (a) TLP structure consisting of four cylindrical columns on box-type pontoons and (b) column-pontoon connection structure with target local structure (bracket girder)

the eigenvalue analysis with maximum deflection of 3.5 mm in the out-of-plane direction (Z-direction). The reference global load $\boldsymbol{f}_r^g$ is selected as 1/100 of the applied loads

Fig. 18(a) shows the normalized second variation of the strain energy with respect to the target local structure calculated at each global load ratio (λ_i^g). The bracket girder is stable until the global load ratio reaches $\lambda_i^g = 3.5$. Fig. 18(b) shows the deformed shapes and plastic regions of the target local structure when the global load ratios are $\lambda_i^g = 1.0, 2.0, 3.1, 3.5, 3.8,$ and 4.0. The first yielding occurs at $\lambda_i^g = 2.0$ and more than 70% of the target local structure is subjected to plastic deformation at $\lambda_i^g = 4.0$.

Fig. 19 shows the local force ratio λ_i^l with respect to the global load ratio (λ_i^g) at each load step i. The critical global load and local force ratios can be determined as $\lambda_c^g = 3.5$ and $\lambda_c^l = 3.22$, respectively. After the critical point, the local force ratio considerably decreases. Using Eqs. (8) and (9), the usage factor and the local safety factor are calculated as $\eta = 0.31$ and $LSF = 3.22$ when the service load ratio is considered to be $\lambda_s^l = 1.0$. Fig. 20(a) shows the node sequence over the boundary of the target local structure, and Figs. 20(b)-(c) compare the components of the applied local forces ($\boldsymbol{f}_i^l$) and the approximated local

force ($\lambda_i^l \boldsymbol{f}_r^l$) at the critical point.

The displacement index-local force ratio curve is plotted as illustrated in Fig. 21. After the critical point ($\lambda_c^l = 3.22$), softening occurs in the target local structure. For comparison, the global load ratio-normalized displacement index curve is plotted as shown in Fig. 22. The results in Fig. 22 indicate that the global structure is stable at the critical point ($\lambda_c^l = 3.22$) as the applied global load continuously increases as the displacement increases. Comparing Fig. 21 and Fig. 22, the locally unstable state cannot be observed by investigating the global response of the structure, but the proposed methods predict the local instability in the target local structure well.

4. Conclusions

In this study, we proposed three different methods to evaluate the stability of a local structural part belonging to a large structure. Through nonlinear FE analysis regarding the global structure, complicated interactions between the local and global structures are directly considered. The methods can be easily used to determine vulnerable areas in a large structure regardless of the shape of the target local structure. The critical point at which the local structure loses its
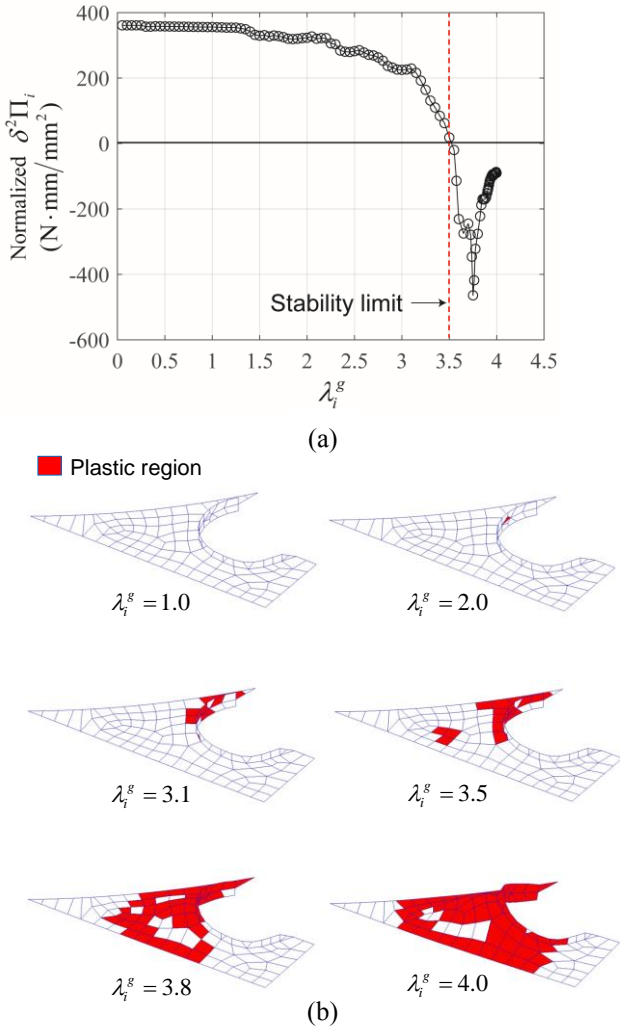
(a)

(b)

Fig. 18 Stability limit determined by relation between global load ratio and second variation of strain energy and stress distribution at the critical point, and plastic deformations in target local structure: (a) normalized second variation of strain energy of target local structure and (b) plastic regions over deformed shapes of target local structure when global load ratios are $\lambda_i^g = 1.0, 2.0, 3.1, 3.5, 3.8,$ and 4.0
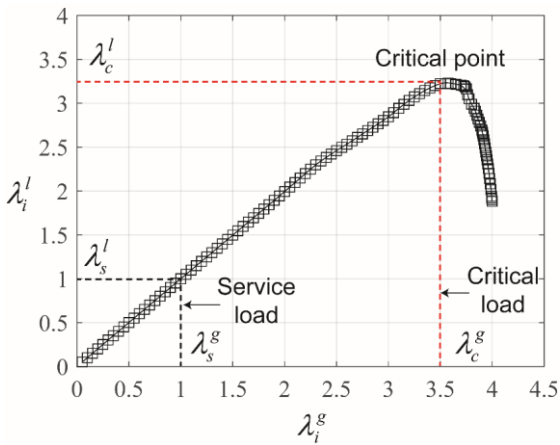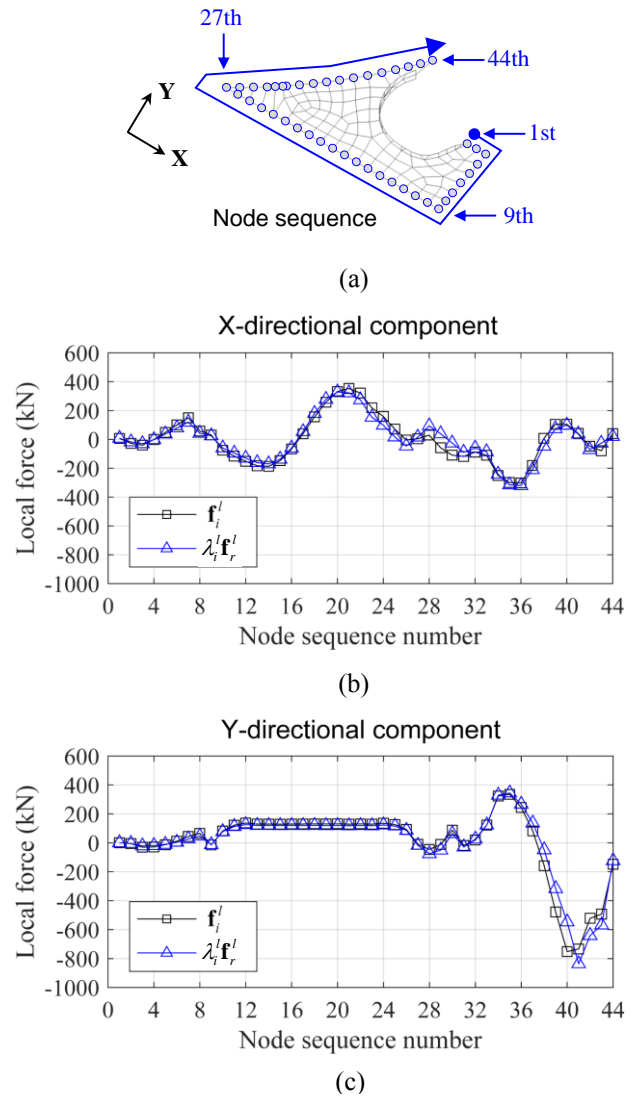

(a)

(b)

(c)

Fig. 20 Comparison between applied and approximated local forces in stiffened cylindrical shell structure: (a) node sequence over interface boundary of target local structure, (b) *X*-directional components of applied and approximated local forces, and (c) *Y*-directional components of applied and approximated local forces

Fig. 19 Global load ratio-local force ratio curve obtained for column-pontoon connection structure of tension leg platform
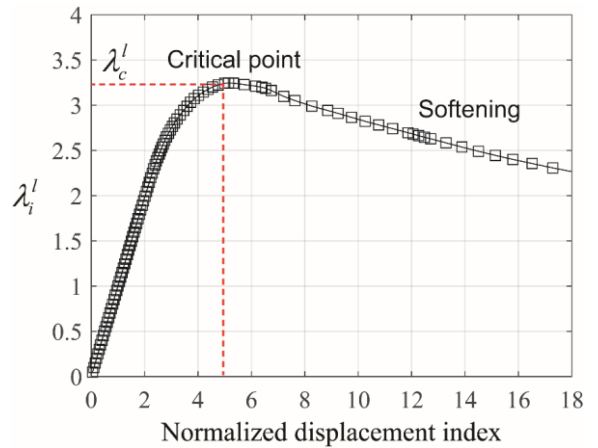

Fig. 21 Normalized displacement index-local force ratio curve obtained for column-pontoon connection structure of tension leg platform
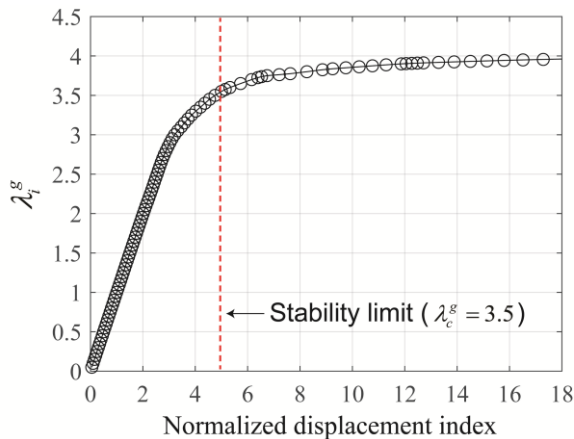
Fig. 22 Normalized displacement index-global load ratio curve obtained for column-pontoon connection structure of tension leg platform

stability can be explicitly found, even if the overall structural integrity is maintained. The resistance capacity of the local structure can be reasonably quantified using the local safety factor (*LSF*).

In future studies, the proposed methods can be applied to demonstrate strength proofs of irregularly reinforced structures and weakened plate openings, which frequently need to be evaluated in the ship building industry but are not predefined in the design formulas. In addition, the residual strength of the local structure can be identified after structural damages occur from ship grounding or collision accidents. The methods can be practically used by engineers to consider various arbitrary shapes of local structural parts in ships and offshore structures.

Acknowledgments

References

ABS (2018), Guide for Buckling and Ultimate Strength Assessment for Offshore Structures, American Bureau of Shipping, New York, U.S.A.

AISC (2016), ANSI/AISC 360-16, An American National Standard: Specification for Structural Steel Buildings, American Institute of Steel Construction, Chicago, U.S.A.

API (2014), RP 2A-WSD, Recommended Practice for Planning, Designing and Constructing Fixed Offshore Platforms- Working Stress Design, American Petroleum Institute, Washington, U.S.A.

Bazant, Z.P. and Cedolin, L. (1991), *Stability of Structures: Elastic, Inelastic, Fracture, and Damage Theories*, Oxford University Press, New York, U.S.A.

Bisagni, C. and Vescovini, R. (2009), "Analytical formulation for local buckling and post-buckling analysis of stiffened laminated panels", *Thin Wall. Struct.*, **47**(3), 318-334. https://doi.org/10.1016/j.tws.2008.07.006.

Blarez, E. (2018), "Moho Nord, a complex integrated project", *Offshore Technol. Conf. Asia*, Kuala Lumpur, Malaysia, March. https://doi.org/10.4043/28406-ms.

Brubak, L. and Hellesland, J. (2007), "Approximate buckling strength analysis of arbitrarily stiffened, stepped plates", *Eng. Struct.*, **29**(9), 2321-2333. https://doi.org/10.1016/j.engstruct.2006.12.002.

Brubak, L., Hellesland, J. and Steen, E. (2007), "Semi-analytical buckling strength analysis of plates with arbitrary stiffener arrangements", *J. Constr. Steel Res.*, **63**(4), 532-543. https://doi.org/10.1016/j.jcsr.2006.06.002.

BV (2018), Rule Note NI 615 DT R02 E, Buckling Assessment of Plated Structures, Bureau Veritas, Paris, France.

DNV (2010), DNV-RP-C201, Recommended Practice: Buckling Strength of Plated Structures, Det Norske Veritas, Oslo, Norway.

DNVGL (2015), DNVGL-CG-0128, Class Guideline: Buckling, DNVGL, Oslo, Norway.

DNVGL (2017), DNVGL-RP-C202, Recommended Practice: Buckling Strength of Shells, DNVGL, Oslo, Norway.

DNVGL (2018), DNVGL-RU-SHIP Pt.3 Ch.8, Rules for Classification: Buckling, DNVGL, Oslo, Norway.

Jamshidi, S. and Fallah, N. (2019), "Buckling analysis of arbitrary point-supported plates using new hp-cloud shape functions", *Struct. Eng. Mech.*, **70**(6), 711-722. https://doi.org/10.12989/sem.2019.70.6.711.

Jaunky, N., Knight, N.F. and Ambur, D.R. (1995a), "Buckling analysis of general triangular anisotropic plates using polynomials", *AIAA J.*, **33**(12), 9387-2654. https://doi.org/10.2514/3.13000.

Jaunky, N., Knight, N.F. and Ambur, D.R. (1995b), "Buckling of arbitrary quadrilateral anisotropic plates", *AIAA J.*, **33**(5), 938-944. https://doi.org/10.2514/3.12512.

Jeon, H.M., Lee, P.S. and Bathe, K.J. (2014), "The MITC3 shell finite element enriched by interpolation covers", *Comput. Struct.*, **134**, 128-142. https://doi.org/10.1016/j.compstruc.2013.12.003.

Jeon, H.M., Lee, Y., Lee, P.S. and Bathe, K.J. (2015), "The MITC3+ shell element in geometric nonlinear analysis", *Comput. Struct.*, **146**, 91-104. https://doi.org/10.1016/j.compstruc.2014.09.004.

Kim, B.J., Park, Y.M., Kim, K. and Choi, B.H. (2019), "Web bend-buckling strength of plate girders with two longitudinal web stiffeners", *Struct. Eng. Mech.*, **69**(4), 383-397. https://doi.org/10.12989/sem.2019.69.4.383.

Kim, D.K., Poh, B.Y., Lee, J.R. and Paik, J.K. (2018a), "Ultimate strength of initially deflected plate under longitudinal compression: Part I=An advanced empirical formulation", *Struct. Eng. Mech.*, **68**(2), 247-259. https://doi.org/10.12989/sem.2018.68.2.247.

Kim, H.S., Park, Y.M., Kim, B.J. and Kim, K. (2018b), "Numerical investigation of buckling strength of longitudinally stiffened web of plate girders subjected to bending", *Struct. Eng. Mech.*, **65**(2), 141-154. https://doi.org/10.12989/sem.2018.65.2.141.

Kim, J.H., Jeon, J.H., Park, J.S., Seo, H.D., Ahn, H.J. and Lee, J.M. (2015), "Effect of reinforcement on buckling and ultimate strength of perforated plates", *Int. J. Mech. Sci.*, **92**, 194-205. https://doi.org/10.1016/j.ijmecsci.2014.12.016.

Kim, U.N., Choe, I.H. and Paik, J.K. (2009), "Buckling and ultimate strength of perforated plate panels subject to axial compression: experimental and numerical investigations with design formulations", *Ship. Offshore Struct.*, **4**(4), 337-361. https://doi.org/10.1080/17445300902990606.

Ko, Y., Lee, P.S. and Bathe, K.J. (2016), "The MITC4+ shell element and its performance", *Comput. Struct.*, **169**, 57-68. https://doi.org/10.1016/j.compstruc.2016.03.002.

Ko, Y., Lee, P.S. and Bathe, K.J. (2017), "A new MITC4+ shell element", *Comput. Struct.*, **182**, 404-418. https://doi.org/10.1016/j.compstruc.2016.11.004.

Komur, M.A. and Sonmez, M. (2008), "Elastic buckling of perforated plates subjected to linearly varying in-plane loading", *Struct. Eng. Mech.*, **28**(3), 353-356. https://doi.org/10.12989/sem.2008.28.3.353.

Lee, P.S. and Bathe, K.J. (2005), "Insight into finite element shell discretizations by use of the "basic shell mathematical model"", *Comput. Struct.*, **83**, 69-90. https://doi.org/10.1016/j.compstruc.2004.07.005.

Lee, P.S. and Bathe, K.J. (2010), "The quadratic MITC plate and MITC shell elements in plate bending", *Adv. Eng. Softw.*, **41**(5), 712-728. https://doi.org/10.1016/j.advengsoft.2009.12.011.

Lee, P.S., Noh, H.C. and Bathe, K.J. (2007), "Insight into 3-node triangular shell finite elements: the effects of element isotropy and mesh patterns", *Comput. Struct.*, **85**, 404-418. https://doi.org/10.1016/j.compstruc.2006.10.006.

Lee, S.E., Thayamballi, A.K. and Paik, J.K. (2015), "Ultimate strength of steel brackets in ship structures", *Ocean Eng.*, **101**, 182-200. https://doi.org/10.1016/j.oceaneng.2015.04.030.

Lee, Y., Lee, P.S. and Bathe, K.J. (2014), "The MITC3+ shell element and its performance", *Comput. Struct.*, **138**, 12-23. https://doi.org/10.1016/j.compstruc.2014.02.005.

Lei, Y., Chen, S., Wang, L. and Xu, H. (2018), "Global strength analysis of a monocolumn FPSO", *Proc. Int. Offshore Polar Eng. Conf.*, Sapporo, Japan, June.

Mohammadzadeh, B., Choi, E. and Kim, W.J. (2018), "Comprehensive investigation of buckling behavior of plates considering effects of holes", *Struct. Eng. Mech.*, **68**(2), 261-275. https://doi.org/10.12989/sem.2018.68.2.261.

MSC Software (2018), MSC Nastran 2018 Quick Reference Guide, MSC Software, Newport Beach, U.S.A.

Muhammad, T. and Singh, A.V. (2005), "The buckling of rectangular plates with opening using a polynomial method", *Struct. Eng. Mech.*, **21**(2), 151-168. https://doi.org/10.12989/sem.2005.21.2.151.

Oh, M.H. (2020), "A practical method for evaluating stability of local structures using strain energy variation", Ph.D. Dissertation, Korea Advanced Institute of Science and Technology, Daejeon.

Pei, Z., Iijima, K., Fujikubo, M., Tanaka, S., Okazawa, S. and Yao, T. (2015), "Simulation on progressive collapse behaviour of whole ship model under extreme waves using idealized structural unit method", *Marine Struct.*, **40**, 104-133. https://doi.org/10.1016/j.marstruc.2014.11.002.

Saad-Eldeen, S., Garbatov, Y.C. and Soares, G. (2016), "Experimental strength assessment of thin steel plates with a central elongated circular opening", *J. Constr. Steel Res.*, **118**, 135-144. https://doi.org/10.1016/j.jcsr.2015.11.005.

Saadatpour, M.M., Azhari, M. and Bradford, M.A. (1998), "Buckling of arbitrary quadrilateral plates with intermediate supports using the Galerkin method", *Comput. Meth. Appl. Mech. Eng.*, **164**(3-4), 297-306. https://doi.org/10.1016/S0045-7825(98)00030-9.

Tham, L.G. and Szeto, H.Y. (1990), "Buckling analysis of arbitrarily shaped plates by spline finite strip method", *Comput. Struct.*, **36**(4), 729-735. https://doi.org/10.1016/0045-7949(90)90087-I.

Wang, C.M. and Liew, K.M. (1994), "Buckling of triangular plates under uniform compression", *Eng. Struct.*, **16**(1), 43-50. https://doi.org/10.1016/0141-0296(94)90103-1.

Wang, D. and Abdalla, M.M. (2015), "Global and local buckling analysis of grid-stiffened composite panels", *Compos. Struct.*,

119, 767-776. https://doi.org/10.1016/j.compstruct.2014.09.050.

Wu, L. and Feng, W. (2003), "Differential cubature method for buckling analysis of arbitrary quadrilateral thick plates", *Struct. Eng. Mech.*, **16**(3), 259-274. https://doi.org/10.12989/sem.2003.16.3.259.

Xiang, Y. (2002), "Buckling of triangular plates with elastic edge constraints", *Acta Mech.*, **156**(1-2), 63-77. https://doi.org/10.1007/BF01188742.

Xiang, Y., Wang, C.M., Kitipornchai, S. and Liew, K.M. (1994), "Buckling of triangular Mindlin plates under isotropic in-plane compression", *Acta Mech.*, **102**(1-4), 123-135. https://doi.org/10.1007/BF01178522.

Zi, G., Kim, H.H., Ahn, J.Y. and Oh, M.H. (2017), "Evaluation of buckling strength of non-structured plates by using the deformation energy", *J. Korea Inst. Struct. Mainten. Inspect.*, **21**(3), 102-113. https://doi.org/10.11112/jksmi.2017.21.3.102.

CC